Causes of glacier melt extremes in the Alps since 1949

Emmanuel Thibert, Pascal Alain Dkengne Sielenou, V. Vionnet, Nicolas Eckert, C. Vincent

AGU PUBLICATIONS

Geophysical Research Letters

RESEARCH LETTER
10.1002/2017GL076333

Key Points:
- Glacier melt follows extreme value statistics if nonstationarity is accounted for
- Global radiation, the latent heat flux, and the amount of snow at the beginning of the melting season are three independent controls of melt variability
- Extremes are ruled by large deviations in global radiation combined with sensible heat; long-wave irradiance and latent heat flux are involved in long-term trends

Supporting Information:
- Supporting Information S1

Correspondence to:
E. Thibert,
emmanuel.thibert@irstea.fr

Citation:
Thibert, E., Dkengne Sielenou, P., Vionnet, V., Eckert, N., & Vincent, C. (2018). Causes of glacier melt extremes in the Alps since 1949. *Geophysical Research Letters*, *45*, 817–825. https://doi.org/10.1002/2017GL076333

Received 9 NOV 2017
Accepted 10 JAN 2018
Accepted article online 16 JAN 2018
Published online 30 JAN 2018

Causes of Glacier Melt Extremes in the Alps Since 1949

E. Thibert[1], P. Dkengne Sielenou[1], V. Vionnet[2,3], N. Eckert[1], and C. Vincent[4]

[1]Université Grenoble Alpes, Irstea, UR ETGR, Saint-Martin-d'Hères, France, [2]Météo-France-CNRS, CNRM, CEN, UMR 3589, Grenoble, France, [3]Centre for Hydrology, University of Saskatchewan, Saskatoon, Saskatchewan, Canada, [4]IGE, Université Grenoble Alpes CNRS, Grenoble, France

Abstract Recent record-breaking glacier melt values are attributable to peculiar extreme events and long-term warming trends that shift averages upward. Analyzing one of the world's longest mass balance series with extreme value statistics, we show that detrending melt anomalies makes it possible to disentangle these effects, leading to a fairer evaluation of the return period of melt extreme values such as 2003, and to characterize them by a more realistic bounded behavior. Using surface energy balance simulations, we show that three independent drivers control melt: global radiation, latent heat, and the amount of snow at the beginning of the melting season. Extremes are governed by large deviations in global radiation combined with sensible heat. Long-term trends are driven by the lengthening of melt duration due to earlier and longer-lasting melting of ice along with melt intensification caused by trends in long-wave irradiance and latent heat due to higher air moisture.

1. Introduction

Glacier mass changes are recognized as sensitive indicators of climate change over the last 50 years (Gardner et al., 2013; Vaughan et al., 2013). Today, glaciers are melting faster than ever observed in the last decades (Zemp et al., 2015) and recent record-breaking glacier melt values can be attributed both to climate extremes and long-term trends in warming (Benestad, 2004; Gardner et al., 2013) and changes in glacier response to climate. Glacier positive feedback responses to climate change include the decrease in surface albedo as unbalanced glaciers expose long-standing and larger ice surface areas rather than snow to global radiation (Oerlemans, 2001). In addition, glacier surface elevation lowering is a geometric response that also produces positive feedback due to the mass balance altitudinal gradient (Elsberg et al., 2001; Huss et al., 2012; Paul, 2010). Direct and feedback responses to warming thus give rise to long-term trends in glacier melt, shifting the glacier melt probability distribution upward. For the first time, we attempt here to disentangle the causes of record-breaking glacier melt between specific extreme climatic conditions and long-term drift in averages. Such an approach requires time series of melt measurements over several decades to infer extreme value statistics and physically based melt computations to seek physical attribution mechanisms and quantify glacier feedback responses.

The theoretical basis to analyze glacier melt from extreme value statistics is the result of the time system in which glacier mass balance is measured in field surveys (Cogley et al., 2011): in the course of the mass change of a (nontropical) glacier within a year, the summer balance is the maximum of mass loss from the late winter-early spring maximum of mass budget to the late fall-early winter minimum of mass (supporting information Text S2). Conceptually, summer mass balance data then constitutes an annual maxima series (Coles, 2001), for which extreme value theory states that, under mild regularity conditions, the three extreme value distributions—Gumbel, Frechet, and Weibull (Fisher & Tippett, 1928)—are the only possible choices. These three distributions can be combined into one family designated as the generalized extreme value (GEV) distribution (Coles, 2001).

Due to these strong theoretical arguments, extreme value theory is widely used in geosciences (Favier et al., 2016; Gaume et al., 2013; Katz, 2010; Katz et al., 2002), allowing robust extrapolation beyond observational records and fair evaluation of return periods associated with the highest (rarest) observations. However, this theory has never been applied to glacier mass balance series to assess the rareness of mass loss extremes. For this purpose, we propose to analyze the long-term mass balance recorded at Sarennes glacier (Thibert et al., 2013), acknowledged to be of great value for inferring climatic fluctuations at high altitudes in the Alps in the

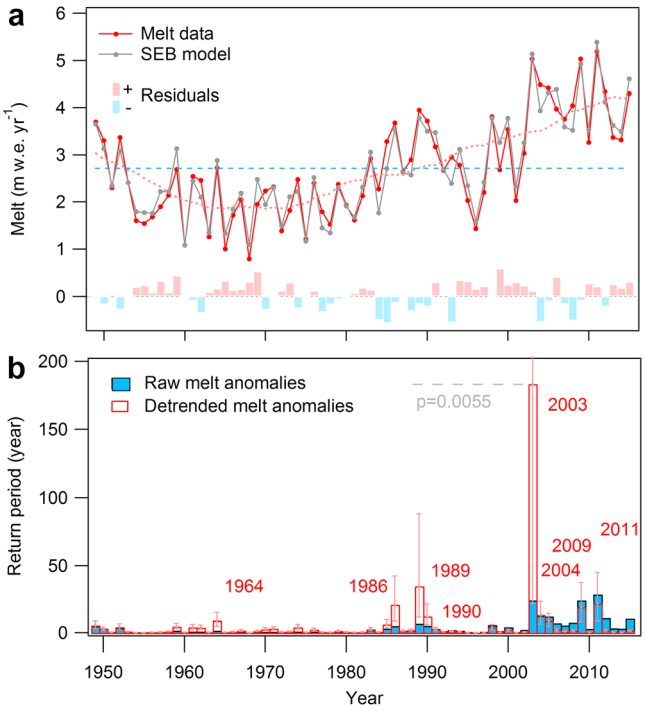

Figure 1. Annual melts and their return period. (a) Time series of annual melt (red line and red dots), long-term 1949–2015 average (blue dashed line), and 21 year moving average (red dashed line). Gray dots are computed melt from the SEB model. Bars are annual residuals between the SEB model and data. (b) Revision of melt return periods using detrended anomalies with the nonstationary hypothesis (red versus blue bars) with computed bootstrap credibility intervals (only displayed for detrended anomalies). The 2003 exceedance probability $p = 0.0055$ year^{-1} corresponds to an event occurring on the average 5–6 times per millennium.

second half of the twentieth century (Thibert et al., 2013; Vincent et al., 2004). Mass balance and melt variations are indeed very similar at the European Alps scale (Letréguilly & Reynaud, 1990; Vincent et al., 2004, 2017); therefore, an analysis from this single glacier should have a wide spatial significance.

2. Data

Sarennes is a south facing glacier (0.09 km^2 in 2015) with a limited altitude range of 150 m between 2,850 and 3,000 m above sea level, located in the Grande Rousses range (45°07′N, 6°07′E, French Alps). Since 1949, systematic winter, and summer mass balance measurements have been carried out, from which annual balances are calculated (Thibert et al., 2013; Text S1). Sarennes provides detailed point-mass balance observations repeated year to year at the same locations, forming one of the longest series worldwide (World Glacier Monitoring Service, 2015; Zemp et al., 2013). Hereafter, melt is considered as a positive quantity, that is, the opposite of summer balance (a loss conventionally defined negatively). We use the term melt in place of summer balance as for glaciers at midlatitudes such as Sarennes, summer mass loss is effectively essentially due to snow and ice melt (Thibert et al., 2013). Sublimation is limited to around 5% of the summer mass loss (Sicart et al., 2008) and can therefore be neglected. Note also that the summer balance can also include some mass input through potential solid precipitation at high elevations in summer (Cogley et al., 2011), a possibility which is accounted for in the surface energy balance analysis.

To limit local topographic effects, we use the time signal free of any feedback from changes in glacier surface area (Huss et al., 2012) as extracted by variance analysis (Eckert et al., 2011), thus revealing the effect of climatic forcing (Huss & Bauder, 2009; Vincent et al., 2017). We used here the variance analysis that was found suitable for Sarennes (Eckert et al., 2011; Lliboutry, 1974) and that states that melt can be decomposed into two independent spatial (α_i) and temporal (β_t) variation terms, giving

$$b_{i,t} = \alpha_i + \beta_t + \varepsilon_{i,t}, \quad (1)$$

where $b_{i,t}$ is the melt recorded at site i for year t, α_i the spatial effects at location i (i.e., the average melt at the site over the whole 1949–2015 study period), and β_t the annual deviation from this average balance (therefore $\Sigma\beta_t = 0$). The spatial-temporal decomposition implies that β_t is the same for each location for any given year t and has a glacier-wide significance. As the melt at each stake only differs from β_t by a constant α, year-to-year variations can be indifferently analyzed through β_t or $\alpha + \beta_t$ (Eckert et al., 2011). We choose the average α_i at stake no. 2 for α (2.71 m water equivalent (mwe) yr^{-1}), providing the mass balance series SMB = $\alpha_2 + \beta_t$ (Figure 1) for further analyses from 1949 to 2015. This stake indeed provides detailed information on snow and ice ablation periods as analyzed with the surface energy balance (SEB) model. Note that this choice has no incidence on the extreme value statics analyses based on the β_t time series.

Regarding the resulting melt time series, trends are clearly visible (Figure 1) and nonstationarity has already been quantitatively assessed (Eckert et al., 2011; Thibert et al., 2013). Therefore, the series considered hereafter will be either raw or detrended (Cleveland, 1977; Text S3).

3. Methods

3.1. Extreme Value Distributions

As melt extreme values are expected to follow GEV distributions according to Fisher and Tippett (1928), we used the framework of extreme value theory for analyzing melt extremes and their return periods (Katz et al.,

2002). The block maxima approach consists of modeling a sequence of maximum values, such as melt anomalies, retrieved from blocks or periods of equal length as the annual melting seasons in our study. The probability distribution of extreme events selected this way converges asymptotically to the (GEV) distribution for which the cumulative distribution function is as follows:

$$P(Z \leq z) = \exp\left\{-\left[1+\xi\frac{(z-\mu)}{\sigma}\right]^{-1/\xi}\right\}, \quad (2)$$

expressing the nonexceedance probability P for the variable Z relative to threshold z. The location parameter μ specifies the position of the center of the distribution, the scale parameter σ determines the magnitude of deviations around the location parameter, and the shape parameter ξ governs the tail behavior of the GEV distribution. The limiting cases of $\xi = 0$ give the Gumbel distribution, while $\xi > 0$ and $\xi < 0$ give, respectively, the Frechet and the Weibull distributions bounded by $\mu - \sigma/\xi$.

Regarding μ, σ, and ξ parameter estimations, for both raw and detrended melt data and under the Frechet/Weibull and Gumbel assumptions, the parameters of the GEV distribution were estimated by likelihood maximization using standard numerical techniques (Brooks, 1998). Bayesian methods were also implemented, providing very similar results and showing the robustness of the obtained estimates. We used the Kolmogorov-Smirnov test to measure the goodness of fit in each case. Parameter standard errors were used to evaluate confidence intervals on return periods using a delta-like uncertainty propagation approach (Coles, 2001; Text S5 and Table S1).

3.2. Surface Energy Balance Model

To seek physical attribution mechanisms in trends and extremes, melt is reconstructed from surface energy balance (SEB) computations. The SEB model was driven by a combination of 1959–2015 Météo-France SAFRAN reanalyses (Dumont et al., 2012; Durand et al., 1993; Durand, Laternser, et al., 2009) and Météo-France homogenized weather data. SAFRAN data limited to 1959–2015 were extended to cover the whole period of Sarennes measurements from parameterizations (Konzelmann et al., 1994; Oerlemans, 1992; Text S6).

The surface energy balance is conceptually calculated from the equilibrium of energy at the glacier surface considering that radiative and sensible heat are balanced by latent heat fluxes associated with mass exchanges due to change of state at the glacier surface. The surface energy balance (SEB) represents the heat content in a control mass unit available for melt. This reads (Oke, 1987)

$$\mathrm{SEB} = S - S + L - L + H + \mathrm{LE} = Q_f \quad = \rho L_f \dot{m}, \quad (3)$$

where $S\downarrow$ is the global radiation (short-wave irradiance), $S\uparrow$ the reflected short-wave radiation, $L\downarrow$ and $L\uparrow$ the long-wave irradiance and emittance, H the turbulent flux of sensible heat, and LE the turbulent latent heat due to sublimation. The net short-wave radiation flux, $S\downarrow - S\uparrow$, can be written $S\downarrow(1-\alpha)$ where α denotes the surface albedo. The long-wave emittance is fixed at 316 W m^{-2} for snow/ice considered to be at the melting point during the entire melting season. As set on the right-hand side of equation (3), the latent energy term related to fusion, Q_f, is conventionally defined as positive and related to melt $\dot{m}$ by the latent heat of fusion L_f and the density ρ of ice.

To estimate sensible and latent heat transfers, the bulk aerodynamic method is used, considering a standard meteorological screen. SAFRAN large-scale wind speed data were corrected to account for topographic effect at the glacier scale (Text S7 and Figure S4d). To define stability conditions in the surface layer, daily means for wind speed and temperature were considered (average bulk Richardson number of 0.0215) (Hartmann, 1994). This corresponds to a stable surface layer under neutral to slightly damped forced convection (Braithwaite, 1995, 2009; Schlögl et al., 2017), and the neutral formulation for the transfer coefficient was therefore applied.

The SEB model was fitted on both snow and ice melt data (Text S8). Glacier surface conditions in 1949 (ice and old firn) were set by mass balance reconstruction from Torinesi et al. (2002). Snow at the beginning of the melting seasons was set as input from the measured winter balance. To account for snow aging, snow albedo was defined daily, decreasing linearly with the snow ablation duration. Three parameters were tuned in the model: two for snow albedo (daily decreasing rate + intercept) and the other for ice albedo.

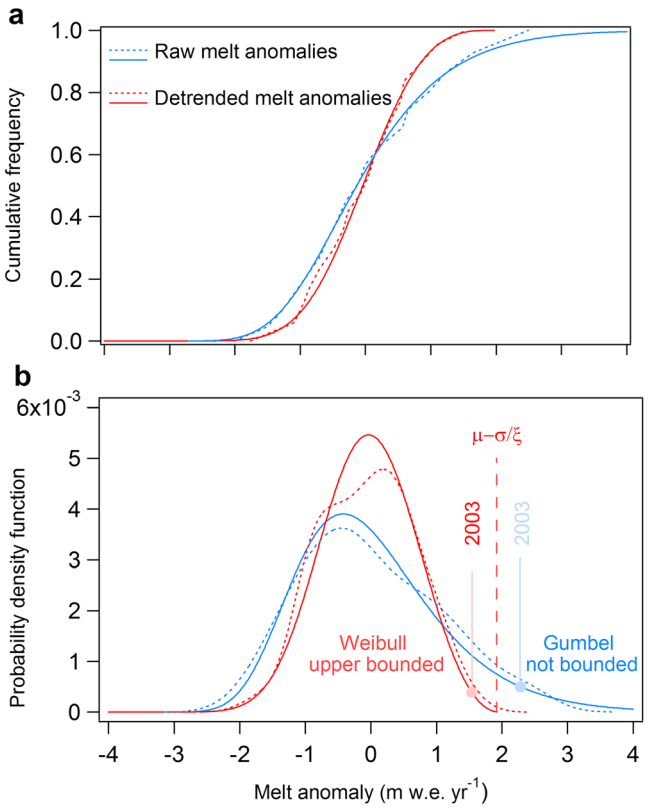

Figure 2. Statistical distribution of melt anomalies. (a) The cumulative distribution function and (b) the probability density function. In both figures, blue curves plot the melt anomalies with respect to the 1949–2015 average assumed as stationary (raw anomalies). The red curves plot the detrended anomalies accounting for nonstationarity. Solid curves show the fit to the GEV distribution and dotted curves show the fitted data. The vertical dashed line in Figure 2b) is the upper bound of the Weibull distribution found when nonstationarity is included (detrended data).

To analyze the links between SEB terms, data dimension reduction was investigated by principal component analysis (PCA) (Husson et al., 2010). This statistical procedure converts possibly correlated variables into a set of values of linearly uncorrelated variables (principal components). Then, similarity and dissimilarity between melting seasons were investigated using agglomerative clustering, and hierarchical trees were considered according to Ward's criteria (incremental clustering; Murtagh & Legendre, 2014; Ward, 1963). Details are provided in the supporting information (Text S10).

4. Results

4.1. Discerning Melt Extremes Within Trends

We first consider raw melt anomalies with respect to the 1949–2015 long-term average (2.71 m of water equivalent in snow and ice melt per year—mwe yr^{-1}). Figures 2a and 2b show the resulting statistical GEV distribution for the cumulative frequency and probability density functions. An unbounded Gumbel-type distribution ($\xi = -0.13 \pm 0.11$) appears to be a good choice (p value = 0.95), avoiding any bounding of the distribution by a theoretical limit. This results in potentially very high values for melt, far above the highest observed values, which may occur with rather common probabilities. Quantitatively, return periods, that is, the expected frequency of exceedance, have been computed (Figure 3) to quantify the average recurrence interval of annual melt maxima (Text S4). A conclusive analysis from Figure 3 is that an extreme melt event such as the one observed in 2003 is assigned to a rather short return period of only 24 years within a relatively narrow (12–49 years) 95% confidence interval. Similar return periods are assigned to 2009 and 2011 (24 years and 28 years) in the late years of the series. The exceptional nature of the 2003 heat wave (Luterbacher et al., 2004) makes these results dubious. Even more physically questionable is the lack of any upper bound in the distribution of melt anomalies resulting from a Gumbel-type distribution and leading to an infinite surface energy balance responsible for melting.

We therefore reconsider the hypothesis of exchangeability of melt years, in order to account for their nonstationarity attributable to climate change over the seven-decade record. We use a 21 year moving average (Figure 1) to compute the long-term trend and detrended annual deviations (Liebmann et al., 2010). Adopting a 31 year detrending window marginally affects anomalies and fitted distributions (Text S3). Figure 2a shows the GEV distribution fitted on detrended melt anomalies (p value = 0.99). This distribution shows distinct characteristics and is inherently different, as its shape parameter characterizes an upper-bounded Weibull-type distribution ($\xi = -0.31 \pm 0.08$).

Figure 1b shows how return periods change for each specific year of the record after assigning them a revised exceedance probability from the new (i.e., accounting for nonstationarity) distribution. The revised return periods of numerous melt events are higher (2003, 1989, 1986, 1964, and 1990). On the other hand, the revised return periods of recent 2004-to-2015 summer melt events are shorter; in particular, the record-breaking 2009 and 2011 summer melts are now no rarer than the melts observed in the 1980s (Figure 3). The systematic long-term rising trend of the most recent years reduces the magnitude of the anomalies, clearly shifting the melt distribution vertically upward. This effect also explains why 1998, which was the twentieth century record year of glacier mass loss, is revised to a "second-rate" 5 year return period. This demonstrates how long-term trends in means have to be accounted for to properly estimate melt extreme frequencies. Note that despite detrending melt data, several occurrences of extremes remain since the 2000s. This could be explained by some residual time dependence in the data, such as memory effects between succeeding years of large mass losses. Plotting β_t versus β_{t-1} in scatter diagram (Text S10 and

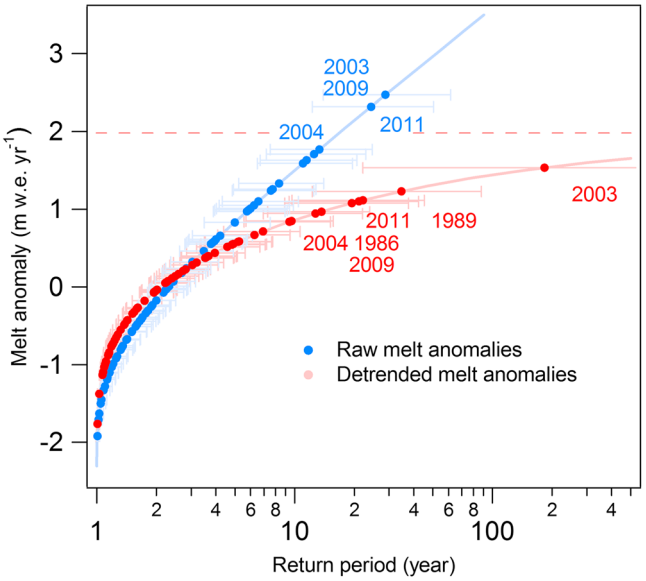

Figure 3. Return periods of melt extremes. For both conditions of stationarity and nonstationarity, blue and red curves plot the melt anomalies (raw or detrended, respectively) as function of their return periods (inverse of the exceedance probability) computed by the distributions fitted to the data. The dots plot return periods assigned by the distribution for each measured melt anomaly with their bootstrap credibility intervals. Note that 2003 and 2009 dots overlap on the blue curve (raw melt anomalies).

Figure S14), this hypothesis is, however, not confirmed, showing no significant correlation (R^2 = 0.12) between detrended melt anomalies. Recent changes in extremes properties that a simple GEV framework cannot account for might be suspected.

With this approach, an event like the 2003 summer melt is very far from the detrended mean (almost 2 times the scale parameter σ) and has a long 183 year return period (p = 0.0055; Figure 1b), much more consistent with the extreme heat wave that affected the European continent and the Alps (Luterbacher et al., 2004) for which the return period was estimated to be up to 500 years (Stott et al., 2004) due to its magnitude and spatial extent. With respect to the seven decades of the series, this resulting return period is not an excessively high estimation—just 3 times the period of record. It nevertheless cannot be excluded that this event could be even rarer considering the very wide (22–7,779 years) computed confidence interval (Figure 3). In such as case, 2003 glacier mass loss could be as rare as the largest historical temperature extremes over several 100 years, such as for instance in the Medieval Warm Period (Glaser et al., 1999; Pfister et al., 1999).

By accounting for nonstationarity, a more physical and realistic bounded behavior is thus obtained to fairly characterize extreme melt value rareness and detrended melt anomalies have an upper limit (μ-σ/ξ = 2 mwe yr^{-1}) that bounds the deviations from the long-term trends. To attribute record-breaking melting to specific extreme climate conditions versus long-term drift in averages and seek physical attribution mechanisms, we reconstructed melt from physically based simulations.

4.2. Modeling the Surface Energy Balance Responsible for Melt

For glaciers such as Sarennes, for which the temperature is at the melting point, snow and ice melt can easily be converted into atmospheric heat fluxes providing the latent heat required for fusion (Paterson, 1994). On the basis of recorded melt durations, melt anomalies are converted into a surface energy balance (SEB). The detailed results of the SEB model can be found in Text S9 of the supporting information. Figures S11a–S11d plot the SEB computation results in mean annual values resulting from daily runs over the 67 ablation seasons. The model fits melt data with 94% of explained variance and within ±0.28 mwe yr^{-1} of RMSE, an acceptable residual with respect to the measurement error range affecting the data (Thibert et al., 2008). The year-to-year variations and links between surface energy components were investigated by principal component analysis (PCA) using five components (Husson et al., 2010): global radiation, long-wave irradiance, sensible heat turbulent flux, latent heat turbulent flux, and winter mass balance, fixing the snow conditions at the beginning of the melting season. The factor map of Figure 4a reports the scatterplot of the 67 surface energy balance reconstructions with respects to the 2 first principal components (Dim.1 and Dim.2). The projection of the components in the space of the two first factors is also reported in the correlation unit circle. All SEB component arrows are close to the unit circle, showing that most of the information is carried by the two first factors (Jolliffe, 1986). Indeed, principal component Dim.1 accounts for 42% of the overall variance and is almost related to global radiation alone. The second component, Dim.2, is uncorrelated (orthogonal) with Dim.1 and nearly a single SEB component as well: the latent heat flux that accounts for 32% of the SEB variance. The third independent component Dim.3 is the winter balance controlling another 19% of melting (Figure 4b). The last factor Dim.4, accounting for a residual 7% of the variance, is not truly attributable to a single SEB term. Almost 74% of the year-to-year SEB variability can therefore be explained mostly by two independent heat fluxes: the global radiation controlling nearly half of the variability of the melting energy and the latent heat flux explaining another third. Sensible heat and long-wave irradiance fluxes are two others energy components, almost independent of each other (R^2 = 0.02), but each related to Dim.1 and Dim.2. The 19% of control by the winter balance on the SEB corresponds to albedo negative feedback from the amount of snow at the beginning of the season. Remarkably, snow precipitation along melting seasons has no effect on seasonal melt (Text S9 and Figure S12).

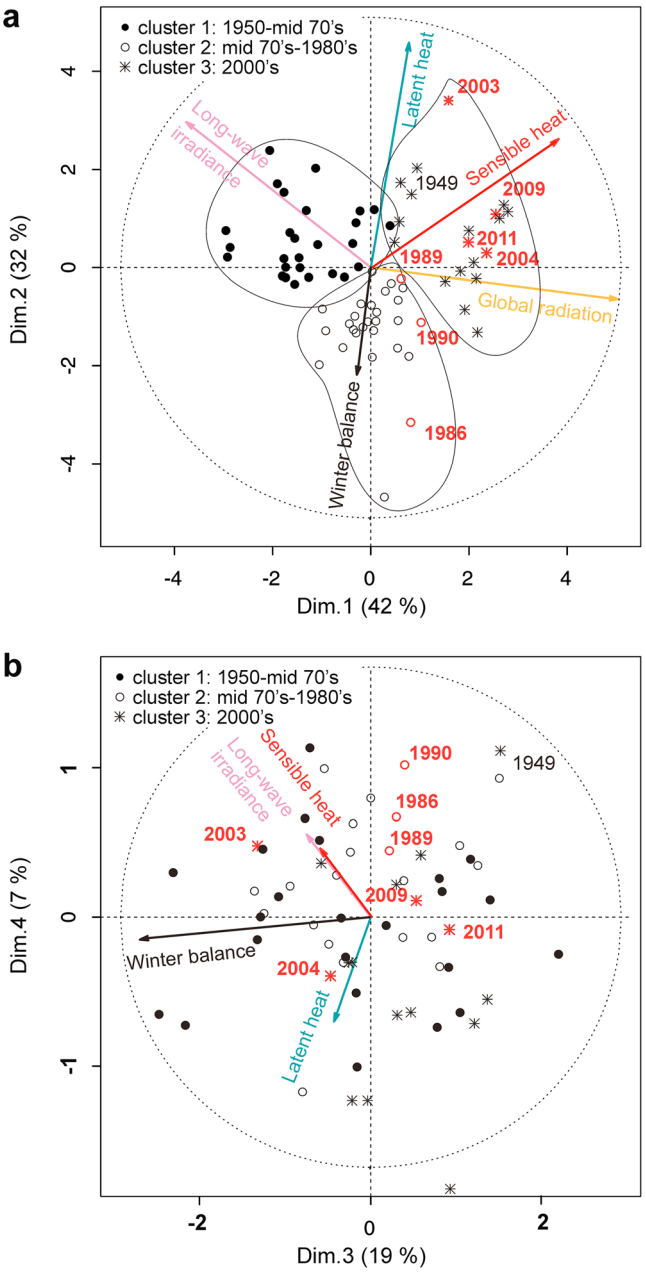

Figure 4. Factors controlling the surface energy balance. Principal components of the energy balance as provided by PCA: (a) Dim.1 is mainly driven by global radiation, and Dim.2 is driven by the latent heat flux. The two heat fluxes account for 74% of the melt variance. (b) Dim.3 is mostly the winter balance, accounting for another 19%. Red markers correspond to melt exceeding the 10 year return period. Melting seasons are plotted with markers corresponding to the three groups identified by the agglomerative clustering.

The PCA is also successful to agglomerates homogeneous melting seasons into clusters (Kaufman & Rousseeuw, 1990) (Figures 4a and S13). This analysis separates clusters into roughly three periods since 1949 and shows three melt regimes (Text S10). Cluster#1 contains especially melting seasons from 1950 to the mid-1970s under high long-wave and low global radiation conditions. Cluster#2 mainly contains the mid-1970s to the 1980s with low turbulent sensible and latent heat flux conditions and low long-wave irradiance. Cluster#3 contains melting conditions driven mostly by high global radiation and sensible and latent heat fluxes in association with higher air moisture conditions as observed since the 2000s. The scatter diagram of Figure 4b shows that the winter balance (Dim.3) is not a variable that contributes to the cluster structure.

Cluster#1 reflects the drift toward lower global radiation (Ohmura, 2009; Ohmura & Lang, 1989) between 1950 and 1980, explained by high cloudiness, and low air temperatures in the European Alps (Auer et al., 2007). Cluster#3 is in line both with brightening in connection to the aerosol content of the atmosphere (Wild et al., 2005) and large sensible heat fluxes in relation to higher air temperatures reported since the 1980s (Philipona et al., 2009). Cluster#3 also contains the 1949 summer season (Figure S13) of remarkably high global radiation, consistent with the 1940s period of enhanced solar radiation reported to explain for instance abnormally high melt rates for glaciers in Switzerland (Huss et al., 2009).

5. Discussion and Conclusions

The top seven melt extremes have systematically occurred under high global radiation, with large turbulent heat fluxes taking part in the 2000s extremes (Figure 4a). Except for 1986, 1989, and 1990, which belong to low turbulent fluxes conditions of Cluster#2 and are explained by very high global radiation alone, melt extremes are related to uncommon high turbulent fluxes in association with strong global radiation (Cluster#3). Most melt extremes are associated with low winter accumulation, except 2003 and 2004 (Figure 4b). Long-wave irradiance is not associated with extreme melt, except to some extent in 2003. This extreme summer melt, which is well simulated (0.13 mwe of model-data discrepancy), is physically explained by the combination of the highest energy fluxes in long-wave irradiance and sensible and latent heat over seven decades. The 2003 simulated SEB has a deviation of +62 W m^{-2} from the seven-decade average. This deviation comes from large deviations in latent heat (+17 W m^{-2}), long-wave irradiance (+15 W m^{-2}), global radiation (+14 W m^{-2}), and sensible heat (+11 W m^{-2}). Deviations in sensible heat and long-wave are linked to the +2.5°C temperature anomaly observed over the 2003 melting season. The deviation in global radiation is related to the low 2003 summer cloudiness (8% below average). The change in turbulent latent heat flux was due to much lower snow and ice sublimation conditions on this specific summer. Those conditions were slightly reversed into atmospheric moisture condensation conditions (positive latent heat, Figure S11c), providing additional heat for melt at the glacier surface. The 2003s melt extreme was nevertheless limited by the winter balance (Figure 4b; in the range of the seven-decade average) that provided a significant amount of snow at the beginning of the season, thereby reducing melt by negative feedback from the albedo.

Summing up, our present results demonstrate that glacier melt follows extreme value statistics if nonstationarity is accounted for, detrending raw observations from two-decade long-term trends in averages that shift distributions. Around this long-term trend, extreme melt anomalies are distributed along an upper-bounded Weibull-type extreme value statistic law. The mean seasonal energy fluxes associated with these melt intensities are reconstructed from a SEB model. Melt deviations and extremes are controlled by three independent drivers: (1) the winter balance determining the amount of snow at the beginning of the melting season, (2) the global (short-wave) radiation giving rise to the largest melt deviations and required for melt extreme occurrences, and (3) the latent heat flux that is controlled by air moisture. Sensible heat is involved in extremes but is a flux connected to latent heat (through wind speed) and global radiation (through air temperature). The long-wave irradiance, varying only slightly and systematically anticorrelated with the net short-wave balances, is not involved in melt extremes.

In light of Thibert et al. (2013), nonstationarity is explained mostly by the lengthening of the ablation season observed since the mid-1980s and also by snow and ice melt intensification in the core of the melting seasons. Regarding the longer ablation seasons, positive feedback from the albedo change due to longer ice versus snow ablation is the main factor. Altitude lowering of the glacier surface accounts here for less than 16% (Thibert et al., 2013) of the trend, but some potential changes in ice albedo cannot be ruled out (Oerlemans et al., 2009). A remarkable finding is that the long-term melt intensification is mainly driven by the latent heat flux increase (+17 W m^{-2}) due to higher air moisture and less snow/ice sublimation, tending to cancel this systematic sink of energy in the SEB. The long-wave irradiance rise (+5 W m^{-2}) is the second factor in melt intensification. It is related to a larger forcing of +3.6 W m^{-2} per decade as assessed by SAFRAN data and consistent with the +2.5 W m^{-2} per decade reported at global scale for the 1990s and 2000s by Ohmura (2012) (Text S9). We expect the long-term trend in melt attributable to the drift in latent heat and long-wave fluxes to continue due to the projected rises in air moisture, greenhouse gases, and higher air temperatures. Projected earlier snowmelt (Musselman et al., 2017), as already reported for seasonal snow cover (Durand, Giraud, et al., 2009), and snow over the glacier accumulation area (Thibert et al., 2013) associated with the lengthening of the ablation season in autumn may increase the ice melt duration and enhance melt from albedo positive feedback. Under increased atmospheric water vapor (Santer et al., 2007), despite more-or-less unchanged relative humidity (Ingram, 2002), snow/ice sublimation together with the associated energy sink of latent heat will be much more limited, providing more energy for melt in the energy balance. More frequent record breaking of glacier melt values should be expected from these upward shifts in SEB averages. Whether future record breakings constitute extreme deviations from averages could be inferred analyzing trends and carrying out GEV analyses. Moreover, potential changes in melt extreme properties cannot be ruled out as already established for temperatures (Schär et al., 2004). For this, a peak over threshold model (Katz et al., 2002) should be tested in place of the GEV approach which supposes steady state for extremes.

Acknowledgments
This study was funded by Observatoire des Sciences de l'Univers de Grenoble (OSUG) and Institut des Sciences de l'Univers (INSU) in the framework of the French "GLACIOCLIM (Les GLACIers comme Observatoire du CLIMat)" project. Irstea Grenoble, CNRM/CEN and IGE are part of Labex Osug@2020. The authors are grateful to M. Zemp and an anonymous reviewer whose comments and suggestions improved the clarity of the manuscript.

References

Auer, I., Jurkovic, A., Lipa, W., Orlik, A., Potzmann, R., Schoener, W., … Nieplova, E. (2007). HISTALP—Historical instrumental climatological surface time series of the greater Alpine region 1760–2003. *International Journal of Climatology*, *27*(1), 17–46. https://doi.org/10.1002/joc.1377

Benestad, R. E. (2004). Record-values, non-stationarity tests and extreme value distributions. *Global and Planetary Change*, *44*(1–4), 11–26. https://doi.org/10.1016/j.gloplacha.2004.06.002

Braithwaite, R. J. (1995). Aerodynamic stability and turbulent sensible-heat flux over a melting ice surface, the Greenland ice sheet. *Journal of Glaciology*, *41*(139), 562–571. https://doi.org/10.1017/S0022143000034882

Braithwaite, R. J. (2009). Calculation of sensible-heat flux over a melting ice surface using simple climate data and daily measurements of ablation. *Annals of Glaciology*, *50*(50), 9–15. https://doi.org/10.3189/172756409787769726

Brooks, S. P. (1998). Markov chain Monte Carlo method and its application. *The Statistician*, *47*, 69–100.

Cleveland, W. S. (1977). Robust locally weighted regression and smoothing scatterplots. *Journal of the American Statistical Association*, *74*, 829–836.

Cogley, J. G., Hock, R., Rasmussen, L. A., Arendt, A. A., Bauder, A., Braithwaite, R. J., … Zemp, M. (2011). *Glossary of glacier mass balance and related terms*. IHP-VII Technical Documents in Hydrology No. 86, IACS Contribution No. 2. Paris: UNESCO-IHP.

Coles, S. (2001). *An introduction to statistical modelling of extreme values*. Berlin: Springer. https://doi.org/10.1007/978-1-4471-3675-0

Dumont, M., Durand, Y., Arnaud, Y., & Six, D. (2012). Variational assimilation of albedo in a snowpack model and reconstruction of the spatial mass-balance distribution of an alpine glacier. *Journal of Glaciology*, *58*(207), 151–164. https://doi.org/10.3189/2012JoG11J163

Durand, Y., Brun, E., Mérindol, L., Guyomarc'h, G., Lesaffre, B., & Martin, E. (1993). A meteorological estimation of relevant parameters for snow models. *Annals of Glaciology*, *18*, 65–71. https://doi.org/10.1017/S0260305500011277

Durand, Y., Giraud, G., Laternser, M., Etchevers, P., Mérindol, L., & Lesaffre, B. (2009). Reanalysis of 47 years of climate in the French Alps (1958–2005): Climatology and trends for snow cover. *Journal of Applied Meteorology and Climatology*, *48*(12), 2487–2512. https://doi.org/10.1175/2009JAMC1810.1

Durand, Y., Laternser, M., Giraud, G., Etchevers, P., Lesaffre, B., & Mérindol, L. (2009). Reanalysis of 44 year of climate in the French Alps (1958–2002): Methodology, model validation, climatology, and trends for air temperature and precipitation. *Journal of Applied Meteorology and Climatology*, *48*(3), 429–449. https://doi.org/10.1175/2008JAMC1808.1

Eckert, N., Baya, H., Thibert, E., & Vincent, C. (2011). Extracting the temporal signal from a winter and summer mass-balance series: Application to a six-decade record at Glacier de Sarennes, French Alps. *Journal of Glaciology*, *57*(201), 134–150. https://doi.org/10.3189/002214311795306673

Elsberg, D. H., Harrison, W. D., Echelmeyer, K. A., & Krimmel, R. M. (2001). Quantifying the effects of climate and surface change on glacier mass balance. *Journal of Glaciolgy*, *47*(159), 649–658. https://doi.org/10.3189/172756501781831783

Favier, P., Eckert, N., Faug, T., & Bertrand, D. (2016). Avalanche risk evaluation and protective dam optimal design using extreme value statistics. *Journal of Glaciology*, *62*(234), 725–749. https://doi.org/10.1017/jog.2016.64

Fisher, R., & Tippett, L. (1928). Limiting forms of the frequency distribution of the largest and smallest member of a sample. *Proceedings of the Cambridge Philosophical Society*, *24*(02), 180–190. https://doi.org/10.1017/S0305004100015681

Gardner, A. S., Moholdt, G., Cogley, J. G., Wouters, B., Arendt, A. A., Wahr, J., … Paul, F. (2013). A reconciled estimate of glacier contributions to seal level rise: 2003–2009. *Science*, *340*(6134), 852–857. https://doi.org/10.1126/science.1234532

Gaume, J., Eckert, N., Chambon, G., Naaim, M., & Bel, L. (2013). Mapping extreme snowfalls in the French Alps using max-stable processes. *Water Resources Research*, *49*, 1079–1098. https://doi.org/10.1002/wrcr.20083

Glaser, R., Brázdil, R., Pfister, C., Dobrovólny, P., Barriendos Vallvé, M., Bokwa, A., … Rodrigo, F. S. (1999). Seasonal temperature and precipitation fluctuations in selected parts of Europe during the sixteenth century. *Climatic Change*, *43*(1), 169–200. https://doi.org/10.1023/A:1005542200040

Hartmann, D. L. (1994). *Global physical climatology*. San Diego, CA: Academic Press.

Huss, M., & Bauder, A. (2009). 20th-century climate change inferred from four long-term point observations of seasonal mass balance. *Annals of Glaciology*, *50*(50), 207–214. https://doi.org/10.3189/172756409787769645

Huss, M., Funk, M., & Ohmura, A. (2009). Strong Alpine glacier melt in the 1940's due to enhanced solar radiation. *Geophysical Research Letters*, *36*, L23501. https://doi.org/10.1029/2009GL040789

Huss, M., Hock, R., Bauder, A., & Funk, M. (2012). Conventional versus reference-surface mass balance. *Journal of Glaciology*, *38*, 278–286.

Husson, F., Lê, S., & Pages, J. (2010). *Exploratory multivariate analysis by example using R*. Computer science and data analysis series. Boca Raton, FL: Chapman and Hall/CRC Press.

Ingram, W. J. (2002). On the robustness of the water vapor feedback: GCM vertical resolution and formulation. *Journal of Climate*, *15*(9), 917–921. https://doi.org/10.1175/1520-0442(2002)015%3C0917:OTROTW%3E2.0.CO;2

Jolliffe, I. T. (1986). *Principal component analysis*. Berlin: Springer-Verlag. https://doi.org/10.1007/978-1-4757-1904-8

Katz, R. W. (2010). Statistics of extremes in climate change. *Climatic Change*, *100*(1), 71–76. https://doi.org/10.1007/s10584-010-9834-5

Katz, R. W., Parlange, M. B., & Naveau, P. (2002). Statistics of extremes in hydrology. *Advances in Water Resources*, *25*(8–12), 1287–1304. https://doi.org/10.1016/S0309-1708(02)00056-8

Kaufman, L., & Rousseeuw, P. J. (1990). *Finding groups in data: An introduction to Cluster analysis*. Hoboken, NJ: John Wiley. https://doi.org/10.1002/9780470316801

Konzelmann, T., van de Wal, R. S.-W., Greuell, W., Bintanja, R., Henneken, E. A.-C., & Abe-Ouchi, A. (1994). Parameterization of global and longwave incoming radiation for the Greenland ice sheet. *Global and Planetary Change*, *9*(1-2), 143–164. https://doi.org/10.1016/0921-8181(94)90013-2

Letréguilly, A., & Reynaud, L. (1990). Space and time distribution of glacier mass-balance in the Northern Hemisphere. *Arctic and Alpine Research*, *22*(1), 43–50. https://doi.org/10.2307/1551719

Liebmann, B., Dole, R. M., Jones, C., Bladé, I., & Allured, D. (2010). Influence of choice of time period on global surface temperature trend estimates. *Bulletin of the American Meteorological Society*, *91*(11), 1485–1492. https://doi.org/10.1175/2010BAMS3030.1

Lliboutry, L. (1974). Multivariate statistical analysis of glacier annual balances. *Journal of Glaciology*, *13*(69), 371–392. https://doi.org/10.1017/S0022143000023169

Luterbacher, J., Dietrich, D., Xoplaki, E., Grosjean, M., & Wanner, H. (2004). European seasonal and annual temperature variability, trends and extremes since 1500. *Science*, *303*(5663), 1499–1503. https://doi.org/10.1126/science.1093877

Murtagh, F., & Legendre, P. (2014). Ward's hierarchical agglomerative clustering method: Which algorithms implement Ward's criterion? *Journal of Classification*, *31*(3), 274–295. https://doi.org/10.1007/s00357-014-9161-z

Musselman, K. N., Clark, M. P., Liu, C., Ikeda, K., & Rasmussen, R. (2017). Slower snowmelt in a warmer world. *Nature Climate Change*, *7*(3), 214–219. https://doi.org/10.1038/nclimate3225

Oerlemans, J. (1992). Climate sensitivity of glaciers in southern Norway: Application of an energy-balance model to Nigardsbreen, Hellstugubreen and Alfotbreen. *Journal of Glaciology*, *38*(129), 223–232. https://doi.org/10.1017/S0022143000003634

Oerlemans, J. (2001). *Glaciers and climate change*. Lisse, Netherlands: Balkema Publishers, A.A./Taylor & Francis Group.

Oerlemans, J., Giessen, R., & van den Broeke, M. (2009). Retreating alpine glaciers: Increased melt rates due to accumulation of dust (Vadret da Morteratsch, Switzerland). *Journal of Glaciology*, *55*(192), 729–736. https://doi.org/10.3189/002214309789470969

Ohmura, A. (2009). Observed decadal variations in surface solar radiation and their causes. *Journal of Geophysical Research*, *114*, D00D05. https://doi.org/10.1029/2008JD011290

Ohmura, A. (2012). Present status and variations in the Arctic energy balance. *Polar Science*, *6*(1), 5–13. https://doi.org/10.1016/j.polar.2012.03.003

Ohmura, A., & Lang, H. (1989). Secular variation of global radiation in Europe. In J. Lenoble & J.-F. Geleyn (Eds.), *IRS'88: Current problems in atmospheric radiation* (pp. 298–301). Hampton, VA: A. Deepak Publishing.

Oke, T. R. (1987). *Boundary layer climates* (2nd ed.). New York: Routledge.

Paterson, W. S. B. (1994). *The physics of glaciers* (3rd ed.). Oxford: Pergamon.

Paul, F. (2010). The influence of changes in glacier extent and surface elevation on modeled mass balance. *The Cryosphere*, *4*(4), 569–581. https://doi.org/10.5194/tc-4-569-2010

Pfister, C., Brazdil, R., Glaser, R., Barriendos, M., Camuffo, D., Deutsch, M., … Rodrigo, F. S. (1999). Documentary evidence on climate in sixteenth-century Europe. *Climatic Change*, *43*(1), 55–110. https://doi.org/10.1023/A:1005540707792

Philipona, R., Behrens, K., Ruckstuhl, C., & C. (2009). How declining aerosols and rising greenhouse gases force rapid warming in Europe since the 1980s. *Geophysical Reseach Letters*, *36*, L02806. https://doi.org/10.1029/2008GL036350

Santer, B. D., Mears, C., Wentz, F. J., Taylor, K. E., Gleckler, P. J., Wigley, T. M. L., … Wehner, M. F. (2007). Identification of human-induced changes in atmospheric moisture content. *Proceedings of the National Academy of Sciences of the United States of America*, *104*, 15,248–15,253.

Schär, C., Vidale, P. L., Lüthi, D., Frel, C., Häberli, C., Liniger, M. A., & Appenzeller, C. (2004). The role of increasing temperature variability in European summer heatwaves. *Nature*, *427*(6972), 332–336. https://doi.org/10.1038/nature02300

Schlögl, S., Lehning, M., Nishimura, K., Huwald, H., Cullen, N., & Mott, R. (2017). How do stability corrections perform in the stable boundary layer over snow? *Boundary-Layer Meteorology*, *165*(1), 161–180. https://doi.org/10.1007/s10546-017-0262-1

Sicart, J. E., Hock, R., & Six, D. (2008). Glacier melt, air temperature, and energy balance in different climates: The Bolivian tropics, the French Alps, and northern Sweden. *Journal of Geophysical Research*, *113*, D24113. https://doi.org/10.1029/2008JD010406

Stott, P. A., Stone, D. A., & Allen, M. R. (2004). Human contribution to the European heatwave of 2003. *Nature*, *432*(7017), 610–614. https://doi.org/10.1038/nature03089

Thibert, E., Blanc, R., Vincent, C., & Eckert, N. (2008). Glaciological and volumetric mass-balance measurements: Error analysis over 51 years for Glacier de Sarennes, French Alps. *Journal of Glaciology*, *54*(186), 522–532. https://doi.org/10.3189/002214308785837093

Thibert, E., Eckert, N., & Vincent, C. (2013). Climatic drivers of seasonal glacier mass balances: An analysis of 6 decades at Glacier de Sarennes (French Alps). *The Cryosphere*, *7*(1), 47–66. https://doi.org/10.5194/tc-7-47-2013

Torinesi, O., Letréguilly, O., & Valla, F. (2002). A century reconstruction of the mass balance of Glacier de Sarennes, French Alps. *Journal of Glaciology*, *48*(160), 142–148. https://doi.org/10.3189/172756502781831584

Vaughan, D. G., Comiso, J. C., Allison, I., Carrasco, J., Kaser, G., Kwok, R., … Zhang, T. (2013). Observations: Cryosphere. In T. F. Stocker, et al. (Eds.), *Climate change 2013: The physical science basis. Contribution of Working Group I to the Fifth Assessment Report of the Intergovernmental Panel on Climate Change* (Chap. 4, pp. 317–382). Cambridge, United Kingdom and New York: Cambridge University Press.

Vincent, C., Fischer, A., Mayer, C., Bauder, A., Galos, S. P., Funk, M., … Huss, M. (2017). Common climatic signal from glaciers in the European Alps over the last 50 years. *Geophysical Research Letters*, *44*, 1376–1383. https://doi.org/10.1002/2016GL072094

Vincent, C., Kappenberger, G., Valla, F., Bauder, A., Funk, M., & Le Meur, E. (2004). Ice ablation as evidence of climate change in the Alps over the 20th century. *Journal of Geophysical Research*, *109*, D10104. https://doi.org/10.1029/2003JD003857

Ward, J. H. (1963). Hierarchical grouping to optimize an objective function. *Journal of the American Statistics Association*, *58*(301), 236–244. https://doi.org/10.1080/01621459.1963.10500845

World Glacier Monitoring Service (2015). In M. Zemp, et al. (Eds.), *Global glacier change bulletin no. 1 (2012–2013)*. Zürich, Switzerland: ICSU(WDS)/ IUGG(IASC)/ UNEP/ UNESCO/ WMO: World Glacier Monitoring Service.

Wild, M., Gilgen, H., Roesch, A., Ohmura, A., Long, C. N., Dutton, E. G., … Tsvetkov, A. (2005). From dimming to brightening: Decadal changes in solar radiation at Earth's surface. *Science*, *308*(5723), 847–850. https://doi.org/10.1126/science.1103215

Zemp, M., Frey, H., Gärtner-Roer, I., Nussbaumer, S. U., Hoelzle, M., Paul, F., … Vincent, C. (2015). Historically unprecedented global glacier decline in the early 21st century. *Journal of Glaciology*, *61*(228), 745–762. https://doi.org/10.3189/2015JoG15J017

Zemp, M., Thibert, E., Huss, M., Stumm, D., Rolstad Denby, C., Nuth, C., … Andreassen, L. M. (2013). Reanalysing glacier mass balance measurement series. *The Cryosphere*, *7*(4), 1227–1245. https://doi.org/10.5194/tc-7-1227-2013